Protein Cell 2013, 4(12): 942–950
DOI 10.1007/s13238-013-3091-0

Protein & Cell

RESEARCH ARTICLE

Crystal structure of the N-terminal ankyrin repeat domain of TRPV3 reveals unique conformation of finger 3 loop critical for channel function

Di-Jing Shi[1*], Sheng Ye[2*], Xu Cao[1], Rongguang Zhang[2]✉, KeWei Wang[1,3,4]✉

[1] Department of Neurobiology, Neuroscience Research Institute, Peking University Health Science Center, Beijing 100191, China
[2] National Laboratory of Biomacromolecules, Institute of Biophysics, Chinese Academy of Sciences, Beijing 100101, China
[3] Department of Molecular and Cellular Pharmacology, State Key Laboratory of Natural and Biomimetic Drugs, Peking University School of Pharmaceutical Sciences, Beijing 100191, China
[4] PKU-IDG/McGovern Institute for Brain Research, Peking University, Beijing 100871, China
✉ Correspondence: rzhang@ibp.ac.cn (R. Zhang), wangkw@hsc.pku.edu.cn (K. W. Wang)
Received August 23, 2013 Accepted October 9, 2013

ABSTRACT

In all six members of TRPV channel subfamily, there is an ankyrin repeat domain (ARD) in their intracellular N-termini. Ankyrin (ANK) repeat, a common motif with typically 33 residues in each repeat, is primarily involved in protein-protein interactions. Despite the sequence similarity among the ARDs of TRPV channels, the structure of TRPV3-ARD, however, remains unknown. Here, we report the crystal structure of TRPV3-ARD solved at 1.95 Å resolution, which reveals six-ankyrin repeats. While overall structure of TRPV3-ARD is similar to ARDs from other members of TRPV subfamily; it, however, features a noticeable finger 3 loop that bends over and is stabilized by a network of hydrogen bonds and hydrophobic packing, instead of being flexible as seen in known TRPV-ARD structures. Electrophysiological recordings demonstrated that mutating key residues R225, R226, Q255, and F249 of finger 3 loop altered the channel activities and pharmacology. Taken all together, our findings show that TRPV3-ARD with characteristic finger 3 loop likely plays an important role in channel function and pharmacology.

KEYWORDS TRPV3, ARD, keratinocyte, 2-APB, skin

INTRODUCTION

Transient receptor potential (TRP) channels are a large family of cation channels that function as cellular sensors for numerous stimuli (Clapham, 2003). According to their sequence homology, TRP channels are divided into seven subfamilies: TRPV, TRPA, TRPN, TRPM, TRPML, TRPP, and TRPC. Among the TRPV subfamily, all six members can be further divided into two groups: the nonselective and heat-activated TRPV1–4 channels primarily expressed in sensory neurons and keratinocytes, and highly Ca^{2+} selective TRPV5–6 channels primarily expressed in epithelial tissues (Montell et al., 2002; Venkatachalam and Montell, 2007). TRPV1–4 channels are activated by temperature, voltage, protons, and chemicals, and are responsible for maintaining homeostasis and sensing environmental changes (Guler et al., 2002; Voets et al., 2004; Caterina, 2007; Dhaka et al., 2009).

TRPV3 can be activated by warm temperature with the threshold about 33°C. TRPV3-knockout mice have deficits in response to innocuous and noxious heat, suggesting the participation of TRPV3 in thermosensation and nociception (Moqrich et al., 2005). Like other TRPV channels, TRPV3 is a multimodal cation channel, and can be activated by natural compounds such as camphor, thymol (Moqrich et al., 2005; Xu et al., 2006), endogenous ligands farnesyl pyrophosphate (FPP), NO (Yoshida et al., 2006; Bang et al., 2010), and a synthetic small molecules 2-APB (Chung et al., 2004a; Hu et al., 2004, 2009). TRPV3 has two distinct features. First, both in native and expression systems, TRPV3 does not desensitize in response to repetitive stimulations (Chung et al., 2004a, 2004b). This property is independent of the stimuli (Moqrich

*These authors contributed equally to the work.

et al., 2005) and is thought to result from sequential reduction of calcium inhibition on TRPV3 from both sides of cells, likely because of conformational changes that occur during successive activation of channel (Xiao et al., 2008a). Second, TRPV3 is abundantly expressed in the keratinocytes of skin containing nerve endings that are physiologically required to respond to physical and chemical stimuli. Consistent with its specific localization, TRPV3 plays critical roles in skin physiology and pathology. TRPV3 knockout mice exhibit wavy hair and curled whiskers (Cheng et al., 2010), likely resulting from misaligned and curved follicles with deranged angles.

TRP channels are assumed to function as tetramers with each subunit containing six transmembrane helices and intracellular N- and C-termini. In the TRPV subfamily, all the six members share conserved ankyrin repeat domains (ARDs) in their N-termini. These ankyrin repeats are involved in protein-protein interactions (Stokes et al., 2005; Kim et al., 2006), channel assembly (Chang et al., 2004; Erler et al., 2004), and trafficking (Arniges et al., 2006). Visualizing the ARDs of TRPV channels is critical for understanding their molecular basis of channel function and regulatory mechanisms. The ARD structures, with or without ATP binding, of several TRPV channels have been reported, including TRPV1, TRPV2, TRPV4, and TRPV6 (Jin et al., 2006; McCleverty et al., 2006; Lishko et al., 2007; Phelps et al., 2008; Auer-Grumbach et al., 2010; Inada et al., 2012). All these structures show that TRPV-ARD contains six ankyrin repeats with each repeat having an anti-parallel helix-turn-helix fold followed by a β-hairpin loop connecting adjacent repeats. The overall fold forms a hand-up shape with the helices as a curved palm and outward projecting loops as fingers. Compared with classical ankyrin repeats, TRPV-ARDs have obvious twists between repeats 4 and 5. In spite of high similarities in overall folds, TRPV-ARDs have apparent differences in hydrophobic surfaces that mediate interactions with regulatory factors (Phelps et al., 2008; Inada et al., 2012). Until now, however, there is no structural information for TRPV3-ARD or other domains available for structural insights into molecular basis of TRPV3 channel function.

In this study, we solved the crystal structure of TRPV3-ARD at 1.95 Å resolution. The structural analysis of TRPV3-ARD reveals six-ankyrin repeats with a long finger 3 loop that differentiates itself from known ARDs of TRPV channels. Patch clamp recordings of TRPV3 mutated in key residues of finger 3 loop confirmed the role of TRPV3-ARD with characteristic finger 3 in channel function and pharmacology.

RESULTS

Overall structure of TRPV3-ARD

The mTRPV3-ARD proteins containing residues 118 to 367 were expressed and purified from Rosetta (DE3) with affinity and size exclusion chromatography (SEC). A single peak of TRPV3-ARD was eluted at elution volume of 16.2 mL, consistent with its molecular weight of 29 kDa, and the protein is monomeric in solution (Fig. 1A). We determined the crystal structure of TRPV3-ARD with molecular replacement by using the structure of rTRPV1-ARD (PDB entry: 2PNN) as a searching model. In the final model of TRPV3-ARD, there are two protein molecules in one asymmetric unit (ASU), which do not dimerize due to the lack of sufficient interactions. The overall crystal structure of TRPV3-ARD reveals a common feature of six ankyrin (ANK) repeats with each repeat consisting of a pair of anti-parallel α-helices and a loop linking the adjacent repeats (Fig. 1B). Since the inner helices pack more tightly than the outer helices, the six repeats stack with a slight counterclockwise twist of about 2–3° along the stacking axis. The overall structure forms the shape of a palm up with outward projecting loops as fingers 1–5 (Fig. 1B). A groove is formed by concave surface of the palm, which can function as binding sites of interacting proteins (Fig. 1B).

TRPV3-ARD shares overall folds with other TRPV-ARD structures, consistent with their high sequence homology among the ARDs of this subfamily. However, several distinct structural features are noted. The most striking variance occurs at finger 3 that bends over towards finger 2 and is stabilized by interactions with inner helix of repeat 3 (Fig. 1C). Other structural differences reside in finger 4 and 5 near the outer helices, where these two fingers are two- and four-residue shorter, respectively, in the sequence of TRPV3-ARD, as compared to TRPV1-ARD. Also, a sequence insertion in TRPV3-ARD causes the loop between outer helix 1 and inner helix 2 to be much longer than that of TRPV1-ARD (Fig. 1C). Because the fingers may function as binding sites in ankyrin groove, these differences suggest the divergence of interacting proteins of different TRPV-ARDs.

The conformation of TRPV3-ARD finger 3

To understand the characteristic conformation of finger 3 in TRPV3-ARD, we made a comparison with previously reported TRPV-ARD structures in which three of them are in complex with ATP (rTRPV1-ARD, cTRPV4-ARD, and hTRPV4-ARD) and four are ligand-free (rTRPV2-ARD, hTRPV2-ARD, hTRPV4-ARD, and mTRPV6-ARD). Since all TRPV-ARD structures share common ANK repeats, the r.m.s.d. among them is in the range of 1.4–1.8 Å for backbone Cαs. However, significant variation in finger 3 conformations suggests that the loop is the most flexible region of TRPV-ARDs (Fig. 2A). Most finger 3 of TRPV-ARDs bear higher B-factors than their adjacent helical regions (Fig. 2B). In fact, the finger 3 of TRPV2-ARD even adopts three different conformations in three different crystal forms, showing its remarkable flexibility (Jin et al., 2006). With or without ATP binding, most finger 3 have no direct interactions with the helices of ANK repeats.

Unlike other TRPV-ARDs, the finger 3 of both TRPV3-ARD molecules in one ASU bends over and forms a unique conformation with appropriate B-factor close to the regions that were not observed in other TRPV-ARDs (Fig. 2B). The bent conformation of the finger 3 in TRPV3-ARD is not due to the crystal packing. We carefully investigated the molecular pack-

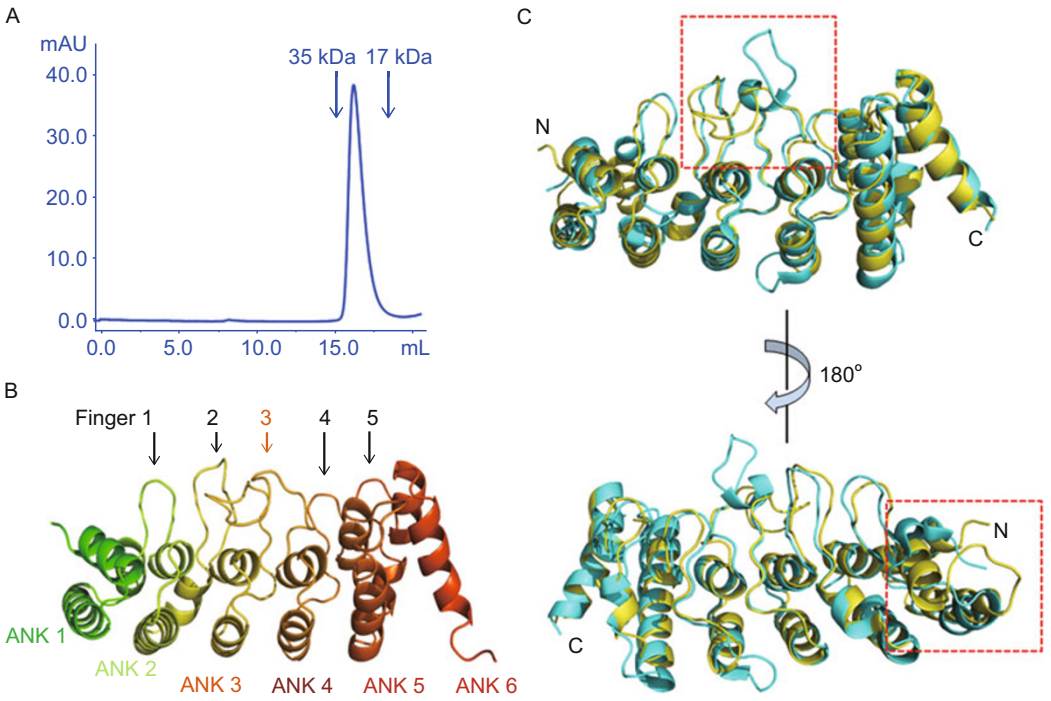

Figure 1. Overall structure of mTRPV3-ARD. (A) Size exclusion chromatography trace of TRPV3-ARD proteins on a Superdex 200 10/300 column. The protein peak represents the absorption at 280 nm with elution volume at 16.2 mL, which is indicated by molecular weights of 35 kDa and 17 kDa, respectively. (B) Ribbon diagram of TRPV3-ARD structure with each repeat and finger numbered and shown in a distinct color. (C) Superposition and comparison of TRPV3-ARD (yellow) and TRPV1-ARD (cyan). Two prominent differences in finger 3 (upper panel) and repeat 1 (lower panel) are shown in red dashed lines, respectively.

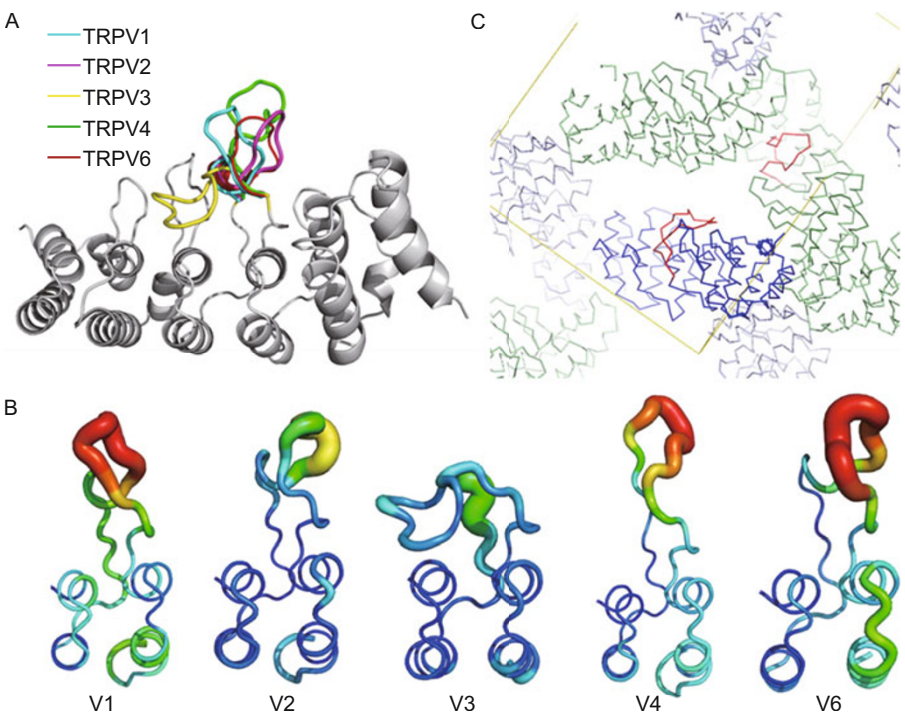

Figure 2. The unique conformation of TRPV3-ARD finger 3. (A) Superposition of the finger 3 in TRPV1–4 and TRPV6 ARDs in different colors with the finger 3 of TRPV3-ARD in yellow. (B) Cartoon putty representation of finger 3 in TRPV1-ARD (PDB entry: 2PNN), TRPV2-ARD (PDB entry: 2F37, chain B), TRPV3-ARD, TRPV4-ARD (PDB entry: 3JXI, chain B), and TRPV6-ARD (PDB entry: 2RFA), with the loop radius proportional to residue B-factors. Only repeat 3 and repeat 4 are shown for clarity. (C) Molecules in the TRPV3-ARD crystal lattice are shown with finger 3 highlighted by red color. One unit cell is indicated by yellow rhomboid.

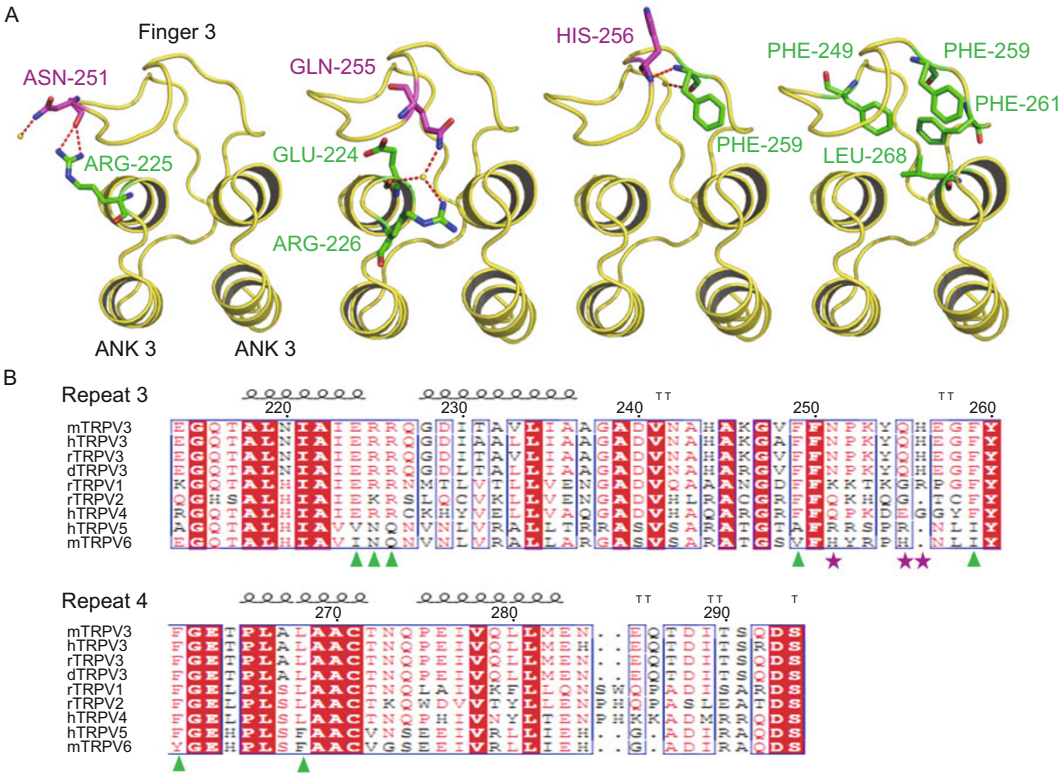

Figure 3. Key residues in finger 3 responsible for stabilizing the conformation of TRPV3-ARD. (A) Hydrogen bonds and hydrophobic packing formed between residues in finger 3 and inner helix of repeat 3 and 4 in TRPV3-ARD. Only repeat 3 and repeat 4 are shown to highlight the residues in interactions. Non-conserved and conserved residues between TRPV1–6 are shown in purple and green color, respectively. (B) Multiple sequence alignments of repeat 3 and repeat 4 between TRPV1–6 from different species. Secondary structure elements are shown above the sequence alignment. Pentagrams (purple) and triangles (green) are indicated as non-conserved and conserved residues in the interactions, respectively.

ing of TRPV3-ARD crystals and noted that there is no contact between finger 3 and TRPV3-ARD molecules around them (Fig. 2C), confirming that its unique conformation is not a result of inter-molecular interactions. In fact, sufficient space can be found near the finger 3 position of both TRPV3-ARDs in one ASU to enable finger 3 to be in an extended conformation.

Instead, the finger 3 in TRPV3-ARD bends to form extensive interactions with the repeats 3 and 4, including several hydrogen bonds and hydrophobic packing, which tightly tethers the usually flexible finger 3 to a stable status. The tip of finger 3 is primarily fixed by hydrogen bonds with the inner helix of repeat 3, where N251 and Q255 of finger 3 and three adjacent residues, E224, R225, and R226, of repeat 3 are involved. The bend of finger 3 is mainly maintained by hydrophobic packing including F249 and F259 from finger3, and F261 and L268 from the inner helix of repeat 4. In addition, a hydrogen bond formed between the main chain atoms of H256 and F259 from finger 3 results in a β-turn, which further maintains the ordered conformation of this usually flexible finger 3 (Fig. 3A). Sequence alignment between repeat 3 and repeat 4 of TRPV1-6 ARDs shows that most residues involved in the interactions between finger 3 and repeat helices are actually highly conserved except residues N251, Q255, and H256 (Fig. 3B). Among them, residue Q255 forms hydrogen bond with a water molecule by its side chain, suggesting that hydrogen bonds fixing the tip of finger 3 are critical for finger 3 bending over, and other interactions make this conformation stable.

The hydrophobic groove in TRPV3-ARD

The sequence alignment shows that there are a number of conserved aromatic residues in TRPV-ARDs. In TRPV3-ARD, there are three and six aromatic residues on finger 2 and finger 3, respectively (Fig. 4A). Analysis of surface electrostatic potentials shows that these aromatic residues form a hydrophobic groove near the twist between repeat 4 and repeat 5, which can function as binding sites for interacting proteins (Fig. 4A). In addition, we noticed that on the surface of TRPV1-ARD bound with ATP there is a positively charged region formed by R115, K155, and K160 interacting with the triphosphate and a ditch that fits the adenine base well. Both the positively-charged region and the ditch are on the surface of TRPV4-ARD (Fig. 4B). Whereas, compared with TRPV1- and TRPV4-ARD, the corresponding positively-charged region of TRPV3-ARD surface

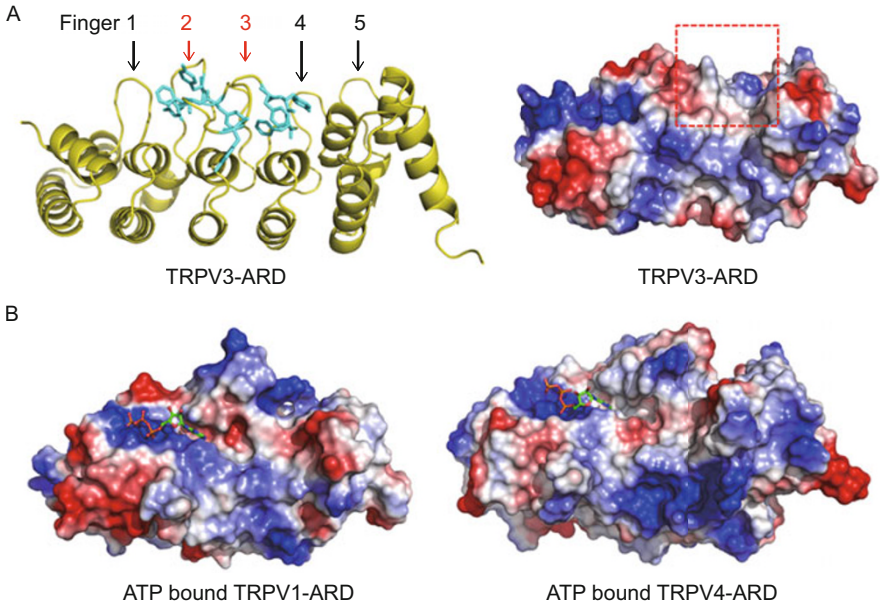

Figure 4. Distinct electrostatic potential surface of TRPV3-ARD. (A) Abundant aromatic amino acids on finger 2 and finger 3 of TRPV3-ARD (left panel) and electrostatic potential surface of TRPV3-ARD (right panel). The hydrophobic groove of TRPV3-ARD is indicated in red dashed lines. (B) Electrostatic potential surfaces of TRPV1-ARD (left panel) and TRPV4-ARD (right panel). Both structures are shown in their ATP bound form. A positive region interacting with the triphosphate and a relatively hydrophobic ditch fitting well with the adenine base can been observed. All electrostatic potential surfaces are calculated using PyMOL (DeLano Scientific, CA, USA).

is much larger, and there is no ditch formed due to the tight conformation of finger 3, indicating at least a different mode of ATP binding than in other TRPV channels, if TRPV3 indeed binds to ATP.

Mutating residues that stablize finger 3 alters channel activity

ARDs in TRPV channels have been reported to be critical in channel assembly, maturation, and trafficking. Alterations in the ARD of TRPV4 cause a spectrum of human skeletal dysplasias and neurodegenerative diseases, resulting from elevated or decreased channel activities (Auer-Grumbach et al., 2010; Landoure et al., 2010). Because the structural feature of TRPV3-ARD finger 3 is distinct, when compared with other TRPV-ARDs, we further tested the role of residues R225, R226, F249, and Q255, responsible for stablizing finger 3 conformation, in channel function. Mutating R225A to disrupt the first hydrogen bond pair, reduced the channel sensitivity to pharmacological opener 2-APB by about three-fold (EC_{50} of 69.9 ± 2 μmol, n = 3), as compared with WT TRPV3 (EC_{50} of 24 ± 2 μmol, n = 3). Double-mutations R226A/Q255A, aimed at breaking the hydrogen bond network, and mutating F249G to disrupt hydrophobic interactions, dramatically increased the sensitivity to 2-APB with EC_{50} 1.5 ± 0.4 μmol (n = 3) and 1.8 ± 0.1 μmol (n = 3), respectively (Fig. 5). These results indicate that conformational changes in finger 3 of TRPV3-ARD altered channel sensitivity to chemical stimulation.

DISCUSSION

In the present study, the goal was to visualize the structure of TRPV3-ARD and understand its roles in channel function, because mutations in conserved ARDs of TRPV subfamily are known to cause a series of diseases due to altered channel activity. Previous studies show that the ARDs of TRPV5 and TRPV6 are involved in channel tetramerization (Chang et al., 2004; Erler et al., 2004); however, SEC as well as crystallization demonstrates that both ARDs of TRPV5 and TRPV6 are monomers in solution (Phelps et al., 2008). In this study our data demonstrate that TRPV3-ARD protein is monomeric in solution. Therefore, TRPV-ARDs are unlikely directly involved in mediation of channel assembly. However, we cannot rule out the possibility that the ARD of TRPV3 regulates channel assembly through interactions with additional factors.

In TRPV1, ARD regulates the desensitization of the channel by binding different ligands. ATP binding to ARD can sensitize TRPV1 and reduce tachyphylaxis, while calmodulin binding is necessary for calcium dependent inactivation of TRPV1. Interestingly, both ligands bind to ARD on the same site, therefore a model of competitive modulatory desensitization has been put forward (Lishko et al., 2007). The binding sites of ATP and Ca^{2+}-CaM on TRPV1-ARD are found to be conserved in TRPV3 and TRPV4. ATP augments TRPV4 current, similar to the effect on TRPV1 (Phelps et al., 2010). However, the modulatory effect of ATP and CaM on TRPV3 is much different than TRPV1 and TRPV4. Unlike TRPV1 and TRPV4 which are

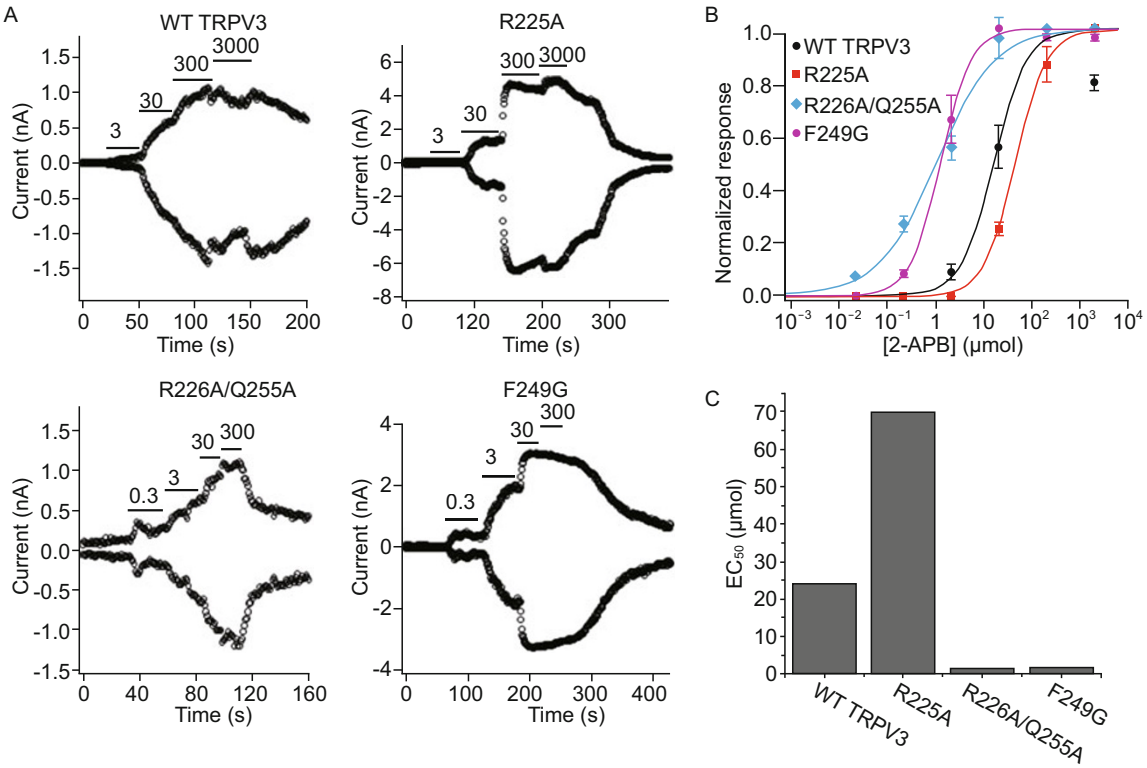

Figure 5. Inside-out patch clamp recordings of HEK293 cells expressing TRPV3 channel and its mutants. (A) Representative currents from inside-out patches in HEK293 cells expressing TRPV3 or mutant channels in response to different concentrations of TRPV3 channel opener 2-APB. (B) Dose-dependent activation of TRPV3 and mutants by 2-APB (black circles: WT; red squares: R225A; blue diamonds: R226A/Q255A; purple circles: F249G). Solid lines represent fits to the Hill equation. (C) EC_{50} values of 2-APB in R225A, R226A/Q255A, and F249G mutants.

desensitized upon repetitive stimulations, TRPV3 is sensitized upon both successive same or different stimuli (Moqrich et al., 2005). It is known that sensitization is due to the decrease of the inhibition by calcium from both sides of cells (Xiao et al., 2008a). In the intracellular side, Ca^{2+}-CaM binds ARD and inhibits TRPV3 current. We speculate that upon repetitive simulations some conformational changes happen, causing a decrease of the affinity between TRPV3 and CaM and an increase of TRPV3 activity. However, the structural basis underlying the sensitivity to repetitive stimulation is still unknown. On the basis of sequence alignment and pull down assay, the binding site of CaM on TRPV3 has been shown to be the same as TRPV1 (Phelps et al., 2010). In the structure of TRPV3-ARD, a stabilized finger 3 may generate steric hindrance which impedes the binding of CaM provided the interaction between CaM and TRPV3 is similar to TRPV1 and TRPV4. Therefore, CaM binding to ARD may induce the conformational change of finger 3, thus resulting in an inhibition of TRPV3 function. Upon successive simulations, the finger 3 of TRPV3-ARD undergoes another conformational change which decreases the binding of CaM, causing the channel to open more easily. In other words, the finger 3 of TRPV3-ARD may function as a switch in regulation of TRPV3 upon ligand binding. Other CaM binding sites of TRPV3 have also been identified (Xiao et al., 2008a), therefore we cannot rule out other domains of TRPV3 interacting with CaM.

Unlike the opposing modulatory effects between ATP and CaM on TRPV1, both ATP and CaM decrease the sensitivity of TRPV3. After the ligand-free apo structure of TRPV3-ARD was obtained, we also tried to co-crystallize TRPV3-ARD with ATP by soaking the crystals in solutions containing different concentrations of ATP and non-hydrolysable ATP analogs ATPγS, ranging from 2.5 mmol/L to 10 mmol/L. Unfortunately, we were unable to obtain any co-crystallizatized structures. Superpositioning of structures between TRPV3-ARD and TRPV1-ARD indicates that the finger 3 in TRPV3-ARD may hinder the binding of ATP. According to the surface electrostatic potential of TRPV3-ARD, there is a positively charged region to interact with the triphosphate of ATP, but the hydrophobic ditch for binding the adenine base of ATP is covered by the bent finger 3, creating a potential steric collision between finger 3 and a ligand such as ATP. We speculate that either ATP binds TRPV3-ARD at a site different from TRPV1-ARD and TRPV4-ARD, or a conformational change of finger 3 is required for exposure of a binding site prior to the binding of ligand ATP.

TRPV-ARDs, with similar biochemical properties and overall conserved structures, can play different roles in channel

regulation. In TRPV subfamily, the cryo-EM structures of both TRPV1 and TRPV4 solved at relatively low resolutions show two regions: a small domain corresponding to the transmembrane portion and a large domain corresponding to the cytoplasmic portion (Moiseenkova-Bell et al., 2008; Shigematsu et al., 2010). The small domains of TRPV1 and TRPV4 are similar in shape, and their transmembrane domains fit well with Kv1.2; however, the large domains between TRPV1 and TRPV4 show prominent differences. In TRPV1, the cytoplasmic domain exhibits a hollow and basket-like shape, connecting to the transmembrane domain with four bridging columns. The ARDs are positioned in a vertical orientation, corresponding to the wall of the basket. While in TRPV4, the ARDs are tilted toward the bridging parts. Because there is no available structure of whole TRPV3, it is difficult to picture the exact position of ARDs in the cytoplasmic domain. However, we speculate that the ARD of TRPV3 is likely to be located differently than TRPV1- and TRPV4-ARD, thus leading to distinct binding of ligands such as ATP and CaM to the ARD of TRPV3 and regulation of the channel activity.

In TRPV4, many mutations in the ARD have been reported to cause a series of inherited diseases, including neuropathies and skeletal dysplasias. Interestingly, mutations associated with neuropathies are mostly located on the convex face of ARD, while mutations causing skeletal dysplasias are primarily on the concave face of ARD (Inada et al., 2012). These mutations affect channel activity, and alter the stability of ARD and ATP binding, but the underlying mechanisms of diseases caused by mutations in the ARD remain unknown. As to TRPV3, G573S, G573C, and W692G substitutions cause the constitutive opening of TRPV3 and lead to Olmsted syndrome (Lin et al., 2012). G573S and G573C substitutions also have been linked to hair loss and spontaneous dermatitis in mice and rats (Xiao et al., 2008b; Yoshioka et al., 2009). However, amino acid substitutions in TRPV3-ARD have not been reported so far and we have little information about the role of ARD in TRPV3 function. In this study, we evaluated three mutations based on the distinct structure of finger 3 of TRPV3-ARD. The R225A mutation leads to decreased channel activity in response to stimulation by 2-APB. In contrast, R226A/Q255A and F249G cause increased channel activity. All these mutations are likely to induce conformational changes in the ARD, thus affecting its interaction with critical regions for alteration of channel activity.

In conclusion, we solved the crystal structure of TRPV3-ARD that features a stable conformation of finger 3 that is likely involved in protein-protein interaction. Mutating residues that disrupt the stability of finger 3 can lead to altered channel activity and pharmacology, implicating a role of ARD in maintaining normal function of TRPV3.

MATERIALS AND METHODS

Subcloning and protein expression

The mTRPV3-ARD coding sequence (residues 118–367) was inserted into *Nde*I and *Xho*I sites of pET21b. The construct included a C-terminal 6× His tag. The protein was expressed in Rosetta (DE3) in LB medium and induced at OD_{600} = 0.8 with 0.5 mmol/L IPTG at 16°C for 18 h.

Protein Purification

Cell pellets were collected by centrifugation at 4000 rpm for 20 min, resuspended in lysis buffer (20 mmol/L Tris-HCl, pH 8.0, 150 mmol/L NaCl) and lysed by sonication. After centrifugation at 18,000 rpm for 30 min, the clear lysate was loaded onto a gravity-flow column containing 2 mL Ni-NTA affinity resin (Qiagen, USA), washed using 20 mmol/L imidazole in lysis buffer and eluted using 500 mmol/L imidazole in lysis buffer. The eluent was desalted to 20 mmol/L by ultrafiltration, then loaded on a sepharose FF column (GE Healthcare) and eluted using a linear NaCl gradient. Fractions containing TRPV3-ARD proteins were concentrated to 0.5 mL and loaded on a Superdex 200 10/300 column (GE Healthcare) in 20 mmol/L Tris-HCl, pH 8.0, 150 mmol/L NaCl. Pure fractions of TRPV3-ARD were concentrated to 15 mg/mL. Typically, the yield was about 7 mg/L of culture.

Electrophysiology

Patch pipettes were pulled from borosilicate glass and fire-polished to a resistance of about 2 MW. Currents were recorded from HEK293 cells expressing mTRPV3 channels in inside-out mode using a HEKA EPC10 amplifier with Patch Master software (HEKA). Both pipette and bath solutions contained 130 mmol/L NaCl, 0.2 mmol/L EDTA, and 3 mmol/L HEPES. Membrane potential was held at 0 mV unless stated otherwise. The voltage stimulation protocol was initiated by a voltage step to +80 mV for 300 ms, followed by a 300 ms step to −80 mV at 1 s intervals. Current amplitude was analyzed at +80 mV. All experiments were conducted at ~22°C. The dose-response relationship was determined using a solution exchanger RSC-200 with seven separate tubing lines to deliver different concentrations of 2-aminoethyl diphenylborinate (2-APB), and current amplitude was recorded.

Crystallization

Purified mTRPV3-ARD proteins were initially crystalized in the condition containing 3.2 mol/L sodium formate, 0.1 mol/L BIS-TRIS propane pH 7.0 when screened with mosquito. Crystals with high quality diffraction datasets were obtained at 25°C by hanging drop vapor diffusion with a 1:1 ratio of protein and reservoir solution (2.4 mol/L sodium formate, 0.1 mol/L BIS-TRIS propane pH 6.4) in each drop. Crystals were flash-frozen after cryo-protection with 15% glycerol in the reservoir solution for future data collection.

Data collection and structure determination

X-ray diffraction data of an mTRPV3-ARD crystal at 100 K were collected at the beamline 19-ID, Advanced Photon Source, Argonne National Laboratory, using a Quantum-315 CCD detector and were processed with HKL2000 (Otwinowski and Minor, 1997). The mTRPV3-ARD structure was determined by molecular replacement with the mTRPV1-ARD structure (PDB entry: 2PNN) as a searching model by using Phenix Phaser. Model refinement and manual adjustment were performed with Phenix Refine (Adams et al., 2010) and COOTs (Emsley and Cowtan, 2004), respectively. Data, phasing, and refinement statistics are listed in Table 1.

Table 1. Data collection and refinement statistics

Data collection	
Wavelength (Å)	0.97930
Resolution range (Å)	50.00–1.95
Data completeness (%)	99.3 (98.3)
Unique reflections	57503
Redundancy	4.0 (3.7)
R_{merge} (%)	8.9 (79.7)
$I/\sigma(I)$	10.5 (1.6)
Refinement statistics	
Resolution range (Å)	42.86–1.95
Space group	$P2_1$
Cell parameters: a, b, c (Å)	61.8, 78.6, 82.9
Cell parameters: β (°)	93.3
r.m.s.d. bonds (Å)	0.016
r.m.s.d. angles (°)	1.6
R_{work}	0.169
R_{free}	0.201

Note: values in parentheses indicate the corresponding statistics in the highest resolution shell.

COORDINATES DEPOSITION

Coordinates of the refined model of TRPV3-ARD and its experimental structural factors have been deposited to Protein Data Bank (http://www.pdb.org/) with the accession number 4N5Q.

ACKNOWLEDGEMENTS

We would like to thank Dr. J Zheng for TRPV3 constructs, suggestions, and discussion for this manuscript. DJS wishes to thank XJ An and Y Zhu for their technical assistance. KWW wishes to thank JM Wang for her consistent support during this research. This work was supported by research grants from the National Natural Science Foundation of China to KWW (Grant Nos. 30970919 and 81221002), and the National Basic Research Program (973 Program) to KWW (No. 2013CB531300).

ABBREVIATIONS

ANK, ankyrin; ARDs, ankyrin repeat domains; ASU, asymmetric unit; FPP, farnesyl pyrophosphate; SEC, size exclusion chromatography

COMPLIANCE WITH ETHICS GUIDELINES

Di-Jing Shi, Sheng Ye, Xu Cao, Rongguang Zhang, and KeWei Wang declare that they have no conflict of interest.

This article does not contain any studies with human or animal subjects performed by the any of the authors.

REFERENCES

Adams, P.D., Afonine, P.V., Bunkoczi, G., Chen, V.B., Davis, I.W., Echols, N., Headd, J.J., Hung, L.W., Kapral, G.J., Grosse-Kunstleve, R.W., et al. (2010). PHENIX: a comprehensive Python-based system for macromolecular structure solution. Acta Crystallogr D Biol Crystallogr 66, 213–221.

Arniges, M., Fernandez-Fernandez, J.M., Albrecht, N., Schaefer, M., and Valverde, M.A. (2006). Human TRPV4 channel splice variants revealed a key role of ankyrin domains in multimerization and trafficking. J Biol Chem 281, 1580–1586.

Auer-Grumbach, M., Olschewski, A., Papic, L., Kremer, H., McEntagart, M.E., Uhrig, S., Fischer, C., Frohlich, E., and Balint, Z. (2010). Alterations in the ankyrin domain of TRPV4 cause congenital distal SMA, scapuloperoneal SMA and HMSN2C. Nat Genet 42, 160–164.

Bang, S., Yoo, S., Yang, T.J., Cho, H., and Hwang, S.W. (2010). Farnesyl pyrophosphate is a novel pain-producing molecule via specific activation of TRPV3. J Biol Chem 285, 19362–19371.

Caterina, M.J. (2007). Transient receptor potential ion channels as participants in thermosensation and thermoregulation. Am J Physiol Regul Integr Comp Physiol 292, R64–76.

Chang, Q., Gyftogianni, E., van de Graaf, S.F., Hoefs, S., Weidema, F.A., Bindels, R.J., and Hoenderop, J.G. (2004). Molecular determinants in TRPV5 channel assembly. J Biol Chem 279, 54304–54311.

Cheng, X., Jin, J., Hu, L., Shen, D., Dong, X.P., Samie, M.A., Knoff, J., Eisinger, B., Liu, M.L., Huang, S.M., et al. (2010). TRP channel regulates EGFR Signaling in Hair Morphogenesis and Skin Barrier Formation. Cell 141, 331–343.

Chung, M.K., Lee, H., Mizuno, A., Suzuki, M., and Caterina, M.J. (2004a). 2-aminoethoxydiphenyl borate activates and sensitizes the heat-gated ion channel TRPV3. J Neurosci 24, 5177–5182.

Chung, M.K., Lee, H., Mizuno, A., Suzuki, M., and Caterina, M.J. (2004b). TRPV3 and TRPV4 mediate warmth-evoked currents in primary mouse keratinocytes. J Biol Chem 279, 21569–21575.

Clapham, D.E. (2003). TRP channels as cellular sensors. Nature 426, 517–524.

Dhaka, A., Uzzell, V., Dubin, A.E., Mathur, J., Petrus, M., Bandell, M., and Patapoutian, A. (2009). TRPV1 is activated by both acidic and basic pH. J Neurosci 29, 153–158.

Emsley, P., and Cowtan, K. (2004). Coot: model-building tools for molecular graphics. Acta Crystallogr D 60, 2126–2132.

Erler, I., Hirnet, D., Wissenbach, U., Flockerzi, V., and Niemeyer, B.A. (2004). Ca2+-selective transient receptor potential V channel architecture and function require a specific ankyrin repeat. J Biol Chem 279, 34456–34463.

Guler, A.D., Lee, H., Iida, T., Shimizu, I., Tominaga, M., and Caterina, M. (2002). Heat-evoked activation of the ion channel, TRPV4. J Neurosci 22, 6408–6414.

Hu, H., Grandl, J., Bandell, M., Petrus, M., and Patapoutian, A. (2009). Two amino acid residues determine 2-APB sensitivity of the ion channels TRPV3 and TRPV4. Proc Natl Acad Sci U S A 106, 1626–1631.

Hu, H.Z., Gu, Q., Wang, C., Colton, C.K., Tang, J., Kinoshita-Kawada, M., Lee, L.Y., Wood, J.D., and Zhu, M.X. (2004). 2-aminoethoxydiphenyl borate is a common activator of TRPV1, TRPV2, and TRPV3. J Biol Chem 279, 35741–35748.

Inada, H., Procko, E., Sotomayor, M., and Gaudet, R. (2012). Structural and biochemical consequences of disease-causing mutations in the ankyrin repeat domain of the human TRPV4 channel. Biochemistry 51, 6195–6206.

Jin, X., Touhey, J., and Gaudet, R. (2006). Structure of the N-terminal ankyrin repeat domain of the TRPV2 ion channel. J Biol Chem 281, 25006–25010.

Kim, S., Kang, C., Shin, C.Y., Hwang, S.W., Yang, Y.D., Shim, W.S., Park, M.Y., Kim, E., Kim, M., Kim, B.M., et al. (2006). TRPV1 recapitulates native capsaicin receptor in sensory neurons in association with Fas-associated factor 1. J Neurosci 26, 2403–2412.

Landoure, G., Zdebik, A.A., Martinez, T.L., Burnett, B.G., Stanescu, H.C., Inada, H., Shi, Y., Taye, A.A., Kong, L., Munns, C.H., et al. (2010). Mutations in TRPV4 cause Charcot-Marie-Tooth disease type 2C. Nat Genet 42, 170–174.

Lin, Z., Chen, Q., Lee, M., Cao, X., Zhang, J., Ma, D., Chen, L., Hu, X., Wang, H., Wang, X., et al. (2012). Exome sequencing reveals mutations in TRPV3 as a cause of Olmsted syndrome. Am J Hum Genet 90, 558–564.

Lishko, P.V., Procko, E., Jin, X., Phelps, C.B., and Gaudet, R. (2007). The ankyrin repeats of TRPV1 bind multiple ligands and modulate channel sensitivity. Neuron 54, 905–918.

McCleverty, C.J., Koesema, E., Patapoutian, A., Lesley, S.A., and Kreusch, A. (2006). Crystal structure of the human TRPV2 channel ankyrin repeat domain. Protein Sci 15, 2201–2206.

Moiseenkova-Bell, V.Y., Stanciu, L.A., Serysheva, II, Tobe, B.J., and Wensel, T.G. (2008). Structure of TRPV1 channel revealed by electron cryomicroscopy. Proc Natl Acad Sci U S A 105, 7451–7455.

Montell, C., Birnbaumer, L., and Flockerzi, V. (2002). The TRP channels, a remarkably functional family. Cell 108, 595–598.

Moqrich, A., Hwang, S.W., Earley, T.J., Petrus, M.J., Murray, A.N., Spencer, K.S.R., Andahazy, M., Story, G.M., and Patapoutian, A. (2005). Impaired thermosensation in mice lacking TRPV3, a heat and camphor sensor in the skin. Science 307, 1468–1472.

Otwinowski, Z., and Minor, W. (1997). Processing of X-ray diffraction data collected in oscillation mode. Method Enzymol 276, 307–326.

Phelps, C.B., Huang, R.J., Lishko, P.V., Wang, R.R., and Gaudet, R. (2008). Structural analyses of the ankyrin repeat domain of TRPV6 and related TRPV ion channels. Biochemistry 47, 2476–2484.

Phelps, C.B., Wang, R.R., Choo, S.S., and Gaudet, R. (2010). Differential regulation of TRPV1, TRPV3, and TRPV4 sensitivity through a conserved binding site on the ankyrin repeat domain. J Biol Chem 285, 731–740.

Shigematsu, H., Sokabe, T., Danev, R., Tominaga, M., and Nagayama, K. (2010). A 3.5-nm structure of rat TRPV4 cation channel revealed by Zernike phase-contrast cryoelectron microscopy. J Biol Chem 285, 11210–11218.

Stokes, A.J., Wakano, C., Del Carmen, K.A., Koblan-Huberson, M., and Turner, H. (2005). Formation of a physiological complex between TRPV2 and RGA protein promotes cell surface expression of TRPV2. J Cell Biochem 94, 669–683.

Venkatachalam, K., and Montell, C. (2007). TRP channels. Annu Rev Biochem 76, 387–417.

Voets, T., Droogmans, G., Wissenbach, U., Janssens, A., Flockerzi, V., and Nilius, B. (2004). The principle of temperature-dependent gating in cold- and heat-sensitive TRP channels. Nature 430, 748–754.

Xiao, R., Tang, J., Wang, C., Colton, C.K., Tian, J., and Zhu, M.X. (2008a). Calcium plays a central role in the sensitization of TRPV3 channel to repetitive stimulations. J Biol Chem 283, 6162–6174.

Xiao, R., Tian, J., Tang, J., and Zhu, M.X. (2008b). The TRPV3 mutation associated with the hairless phenotype in rodents is constitutively active. Cell Calcium 43, 334–343.

Xu, H., Delling, M., Jun, J.C., and Clapham, D.E. (2006). Oregano, thyme and clove-derived flavors and skin sensitizers activate specific TRP channels. Nat Neurosci 9, 628–635.

Yoshida, T., Inoue, R., Morii, T., Takahashi, N., Yamamoto, S., Hara, Y., Tominaga, M., Shimizu, S., Sato, Y., and Mori, Y. (2006). Nitric oxide activates TRP channels by cysteine S-nitrosylation. Nat Chem Biol 2, 596–607.

Yoshioka, T., Imura, K., Asakawa, M., Suzuki, M., Oshima, I., Hirasawa, T., Sakata, T., Horikawa, T., and Arimura, A. (2009). Impact of the Gly573Ser substitution in TRPV3 on the development of allergic and pruritic dermatitis in mice. J Invest Dermatol 129, 714–722.